ELSEVIER

Materials Science and Engineering A347 (2003) 21–31

MATERIALS SCIENCE & ENGINEERING A

www.elsevier.com/locate/msea

Study by X-ray diffraction and mechanical analysis of the residual stress generation during thermal spraying

J. Pina [a,*], A. Dias [b], J.L. Lebrun [c]

[a] Department of Physics, University of Coimbra, P-3004-516 Coimbra, Portugal
[b] Department of Mechanical Engineering, University of Coimbra, Polo II, P-3030 Coimbra, Portugal
[c] LPMI/ENSAM, 2, bd. du Ronceray, BP 3525, F-49035 Angers, France

Received 28 January 2002; received in revised form 28 June 2002

Abstract

Thermally sprayed coatings are formed by the deposition of molten or partially molten particles, propelled onto a substrate where they impact, spread and solidify rapidly. Residual stresses are expected within the sprayed deposit as a consequence of the release of thermal and kinetic energies. A wide range of materials and two spraying techniques are considered in this study, namely atmospheric plasma spraying (APS) and high-velocity oxygen fuel. Stresses were determined by the X-ray diffraction (XRD) method. The results were compared with those calculated by mechanical analysis of stress relief in coatings detached from the substrate. Comparison of the results for adherent and free-standing coatings shows that the residual stress state can be resolved in terms of the components suggested by models that propose two stages of stress generation: quenching stresses and secondary-cooling stresses. The in-depth distribution of residual stresses, through the coating thickness, is discussed in terms of the nature of the coating system.

Keywords: Thermal spray coatings; Atmospheric plasma spraying; High velocity oxygen fuel; Residual stresses; X-ray stress evaluation

1. Introduction

Thermal spraying covers a group of coating technologies characterised by the use of a concentrated and highly energetic heat source, in the form of a flame, plasma jet, shock wave, etc. The metallic or non-metallic, material to be sprayed is delivered to the spray set-up in the form of a powder, rod or wire. It is molten or partially fused and propelled towards the substrate to which the particles adhere mainly by mechanical anchoring. The deposit is built up of successive layers, each one originating in a stream of particles impacting on the target where they spread and solidify rapidly forming splats or lamellae.

This study deals with coatings sprayed by atmospheric plasma spraying (APS) or by high velocity oxygen-fuel (HVOF). The APS technique uses an electric arc established between a tungsten cathode and a water-cooled copper anode as energy source. Depending on the particle size and the physical properties of the material, the powders are completely molten in less than 100 μs and the (alumina) droplets reach velocities in the range 120–180 m s^{-1} at a spray distance of 100 mm [1]. HVOF involves the combustion of oxygen and a fuel gas at high pressure to produce the high-velocity exhaust jet. The heating temperature, which depends on the particular spray gun and the fuel gas used, can reach 3000 K. Sprayed (WC–12Co) particles reach velocities in the range 350–380 m s^{-1} [1], or 300–800 m s^{-1} for stainless steel powders [2]. The APS process mainly transfers thermal energy to the particles, whereas in HVOF the dominant energy transferred is kinetic.

The structure of thermally sprayed coatings is generally characterised by an amount of porosity due to microcracks inside the splats, as well as micropores and very thin gaps between the deposited particles. Non-bonded areas may be formed due to oxidation or non-complete recovery [3–7]. The individual nature of the consolidation and solidification of the droplets leads to

* Corresponding author. Tel.: +351-239-410-641; fax: +351-239-829-158
E-mail address: zepina@ci.uc.pt (J. Pina).

0921-5093/02/$ - see front matter
PII: S0921-5093(02)00580-4

quite different physical and mechanical properties of the coatings compared with those of sintered materials. Studies have shown that interfacial sliding, and microcracking reduce the stiffness of the coatings so that the Young's modulus can be as small as 10% of the bulk value [8,9].

Compared with coatings of the same material sprayed by APS, deposits applied by HVOF exhibit a higher density and higher bond strength due to a higher impact velocity, while the lower combustion temperature leads to a smaller degree of decarbonisation in carbide-containing coatings [1,10].

Important levels of residual stresses are expected in thermally sprayed coatings as a consequence of the high thermal and kinetic energies involved in the process and due to the difference in thermophysical and mechanical properties of substrate and powder materials. The models proposed in the literature to explain residual stress generation can be seen under two perspectives, one focused on individual particles and the other focused in the whole of the deposit. The first has been developed from the earliest studies [3] and is shared by authors who explain the mechanical properties of the coatings by their microstructural characteristics [4,6,11–13]. They consider that the residual stress level is defined in two stages of the process: the deposition, when the sprayed particles strike the target and are quenched to the temperature of the underlying material; and further cooling down to room temperature when the spraying torch is turned-off. This theory is well resumed by Kuroda, who suggests that residual stresses are generated on two scales: the microscopic scale of each sprayed particle and the macroscopic scale of the coating [10].

The second perspective is suggested by authors who propose models based on the thermal history to anticipate the residual stress profile in the depth of the coating [8,14–17]. The effects of general parameters, such as the coating thickness, the substrate temperature, the spray distance, the deposition rate, and others, are studied. Comparison of predictions of such models with experimental data from X-ray diffraction (XRD) [14,16,17], or mechanical methods [5,14,16], shows important deviations. As a consequence, this theory has not been well accepted.

Models that propose two stages for the residual stress generation distinguish between two kinds of stresses, namely transient and residual [3], micro and macro [4], deposition and other [13,18], or quenching and cooling [19]. The former, are generated during the deposition when particles strike the substrate or previously deposited layers. They are explained by the release of the thermal energy involved in the process, and are called quenching stresses [19]. Some authors have also emphasised the effect of the release of kinetic energy and associated it with peening stresses [20]. They suggest that quenching stresses are dominant in processes where the particles are completely molten in the spray gun, as in APS [10]. The particles spread upon impact, but the contraction during cooling and solidification is constrained by the underlying material and tensile stresses are generated inside each sprayed particle. On the other hand, peening stresses are generated in top layers where partially fused particles impact at high velocity, as in HVOF spraying [2,10]. The surface of the target is plastically deformed, inducing a significant level of compressive stresses that add on the previous quenching stresses. Obviously, the surface layer of the coating remains under the effect of the quenching stresses, and the depth of the peening effect was observed to be as deep as 50 μm in 316L stainless steel coatings [2].

The magnitude of such quenching stresses implies that several relaxation mechanisms are activated [4,6,11]. These can include plastic yelding, creep, microcracking and interfacial sliding [21]. The degree of relaxation or the local stress values are not accessible to the experimental measurement, but the effects of the quenching stresses were observed by monitoring the curvature induced in a relatively thin substrate–deposit pair [18,19,22–24]. The results show that the resulting residual stresses are of a level of 10–100 MPa and are insensitive to the substrate material and the spraying conditions, as long as the coating thickness exceeds 10 μm [18], but they are affected by the substrate temperature especially when metallic materials are sprayed [21,25].

The second kind of stresses arise during cooling particularly after spraying; in some of these cases the experiments [18,22] have shown a decrease in the curvature of the specimen or even an inversion of its form. Because they occur during the cooling to room temperature, these stresses were named cooling stresses [19]. They are attributed to the mismatch of thermal expansivity between the coating and substrate materials [10]. As a consequence, they can be either tensile or compressive [12,23]. Although confined to the interface region, the effects can be transmitted along the coating and reach the surface if the deposit structure is compact enough. The magnitude of these stresses is related to the coating and substrate temperatures and to their thermal-expansion coefficients and Young's moduli. These parameters can be quite different from those of the bulk materials [3,4,9,23]. Cooling stresses are also introduced by thermal shock or thermal cycling during service of TBC's (thermal barrier coatings).

The residual stress state in the coatings results, in principle, from the superposition of both mechanisms of stress generation. However, due to the significant implications of the quenching stresses for deposit formation, they are considered by some authors to be the most important source of residual stresses [21]. Thermal mismatch strains between coating and substrate generated later during the cooling to room

temperature can be accommodated in the coating flaws, porosities, or microcracks, and only a limited zone will be affected in the interface with the substrate. The effects of cooling stresses will affect the coatings with a very dense structure, inducing a through thickness residual stress gradient. For such coatings, the residual stress state at the top surface can change from tensile to compressive as the temperature increases, due to different proportions of the quenching and thermal mismatch components [25]. In HVOF sprayed coatings the peening stresses can reach important values, and the residual stress state can be controlled by the spray parameters [2].

XRD, known as X-ray stress evaluation (XSE) when used for stress analysis, is a non-destructive technique, which analyses a surface layer whose thickness depends both on the sample material and the incident beam wavelength. Usually this thickness is not high enough to cover all the depth of a thermally sprayed coating. Nevertheless, this hindrance can be an advantage for studying possible stress gradients in the cross-section by using suitable surface-removal methods or various wavelengths. The technique has extensively been applied to the study of thermally sprayed coatings [9,14,16,17,26–30]. It gives reliable results about the final residual stress state mechanical components while avoiding deposits on thin substrates, or the preparation of special samples to be submitted to layer-removal methods [24,31].

This study focuses on coatings of a wide range of materials sprayed by APS or by HVOF. The goal is to interpret the residual stress values in the framework of the models proposed in the scientific and technological domain of thermal sprayed coatings. For this purpose, the XSE method is used to quantify the residual stresses in the surface layer of coatings adherent to the substrates and also in the depth of some samples. The results are correlated with the microstructure and characteristics of the coatings and compared with values determined at the surface of free-standing coatings. The stresses in the top face of these samples are also estimated by a mechanical method based on the elastic bending of the coating.

2. Materials and methods

2.1. Materials and parameters of the spraying processes

Coatings of several materials were studied to analyse the influence of special characteristics of the microstructure. Coatings of alumina were used to investigate the effects of the bondcoat (NiAl or NiCr) and of the deposit thickness. Coatings of metals and alloys were analysed because the incidence of cracking is usually lower than in ceramic coatings. Cermets, sprayed by HVOF, were studied because of their high density and bond strength.

The technique used to produce each coating was selected according to the sprayed material: APS for the ceramics and HVOF for the metals and cermets. Nevertheless, some exceptions were considered with the aim of studying the particular influence of the spraying process on the microstructure of the deposit. In general, optimised values were chosen for the spraying parameters, as shown in Tables 1 and 2. APS coatings were sprayed with a Castolin Eutectic Eutronic Plasma unit and HVOF coatings were sprayed with a CDS-100 Plasma Technik AG.

Commercial powders were sprayed onto substrates of several materials and thicknesses, as listed in Table 3, where the samples are identified. This table also shows characteristics of the coatings that are significant for the analysis of the residual stress results. Some coatings were deposited in substrates of different thicknesses (e.g. St 37 1.5/5/10 means DIN St 37 K steel with thicknesses of 1.5, 5 and 10 mm). The surface to be coated was previously sandblasted. During spraying the coatings were cooled by directing pressurised air towards the surface. The substrate temperature was not controlled and neither cooling nor pre-heating were usually applied.

2.2. Residual stress analysis

2.2.1. X-ray stress evaluation

Residual stress analysis by XRD was performed with the parameters listed in Table 4, which shows elastic constant values usually found in the literature. Several Kα radiations were used, according to the phase and type of crystalline planes studied in the material. Different thicknesses were studied according to the wavelength used and type of material investigated, as shown in the last two columns of the Table 4. The mean values of the penetration depth were calculated by the formulation given in ref. [32] with X-ray absorption coefficients determined according to [33]. Some mea-

Table 1
Typical APS spraying parameters

	Al_2O_3	NiAl	NiCr	WC–12Co
Primary gas (Ar) flow rate (Nl min^{-1})[a]	10	10	10.6	57
Secondary gas (H_2) flow rate (Nl min^{-1})	11.3	12	7.5	2
Powder feed rate (g min^{-1})	40	60	56	70
Current (A)	700	630	650	530
Voltage (V)	56	63	60	50
Stand-off distance (mm)	125	170	150	130

[a] Flow rate (l min^{-1}) at standard (Normal) atmospheric pressure.

Table 2
Typical HVOF spraying parameters

	$75Cr_3C_225NiCr$	88WC12Co	83WC17Co
Oxygen flow (Nl min^{-1}) [a]	420	420	420
Propane flow-C_3H_8 (Nl min^{-1})	60	55	55
Powder feed rate (g min^{-1})	25	45	38
Spray distance (mm)	300	300	300

[a] Flow rate (l min^{-1}) at standard (Normal) atmospheric pressure.

surements were carried out in depth after removing successive layers of the coating by using a mechanical polishing for ceramics and electropolishing for metals and cermets. The mechanical polishing was performed by using a smooth abrasive paper in such a way that the introduced stresses were lower than the standard deviation of the results. A previous study was carried out in order to check this point. The final results were corrected for the effect of stress relief by using appropriate mechanical models [34]. A linear dependency of $d_{\psi\psi}$ on $\sin^2\psi$ was always observed, thus showing a homogeneous stress–strain distribution within the irradiated area and justifying the use of the classical $\sin^2\psi$ method [35].

The X-ray elastic constants (XEC) were calculated by using the same values and models as for bulk material. This practice was dictated by the conclusions of a previous study where the subject was extensively treated [9].

2.2.2. Analytical estimate of the cooling stresses

The cooling stresses are generated at the interface coating-substrate, due to the differential thermal contraction. They can be approximately estimated by using the equation below [36], under the following assumptions: (i) the deposit thickness is much smaller than the thickness resulting from the assembly formed by the substrate and its holder at the spraying set-up, (ii) the material of the interface coating-substrate has a perfectly elastic behaviour:

$$\sigma_C(T_0) = (\alpha_C - \alpha_S)(T_I - T_0)E_C(T_0) \quad (1)$$

where T_0 is the room temperature, α_C is the coefficient of linear thermal expansion of the coating, α_S is the coefficient of linear thermal expansion of the substrate, T_I is the average temperature in the interface just after the terminus of the spraying process, and E_C is the Young modulus of the coating. The parameters were selected according to the explanations in the following paragraphs.

The value of room temperature was considered to be $T_0 = 25$ °C. The coefficients of linear thermal expansion of the coating and substrate were as those of the same bulk materials. This assumption is supported by the conclusions of several studies usually dealing with the application of coatings as thermal barriers. Values of the order of these for non-sprayed dense material [23,37,38], or even lower [39] are determined. The values used, were taken from the literature are listed in Table 5.

The temperature in the interface coating-substrate was determined by using three thermocouples implanted in the backside of the substrate at distances of 0.5 mm from the interface. It was observed that, when the coating surface was cooled by a jet of compressed air during spraying, the interface temperature was stabilised at a value close to 200 °C. This temperature was reached after some exposure to the plasma torch and remained independent of the coating thickness. According to these considerations, a value of $T_I = 200$ °C was used for the calculation.

The values for $E_C(T_0)$ at room temperature were determined by cantilevered flexure of free-standing coatings, using a technique described elsewhere [9].

2.2.3. Evaluation of the cooling stresses by a mechanical method

This study was carried out on several coatings by measuring the curvature radius of free-standing deposits, after removing the substrates by chemical dissolution. The method assumes that the amount of stresses released by the sample curvature is equivalent and opposite in sign to the stresses induced by the thermal mismatch strains at the coating-substrate interface, during cooling. This means that the maximum bending stress at the top surface of the coating is symmetric to the stress at the interface side, and the neutral axis is located in the mid-plane of the deposit. The calculation is based on the formulation of the elasticity theory giving the stresses-σ-in the top face of a beam subjected to a pure bending moment:

$$\sigma = \frac{E_C}{r} y \quad (2)$$

where E_c is the macroscopic modulus of elasticity of the material, r is the radius of curvature, and y is the distance to the neutral axis. The values of E_c were determined by using free-standing coatings and the method referred to in the previous section. The radius r was measured for each sample by using a computerised profilometer. The value of y was considered to be one half the thickness of the coating.

2.3. General experimental procedures

Microhardness Vickers tests were performed on the polished cross-sections of some samples. To reduce the interaction with porosity, a testing load of 50 g was applied for 15 s. Five measurements were taken to calculate the average value.

Table 3
Samples and their principal characteristics

Sample	Spray process	Substrate material + thickness (mm)	Powder composition (%)	Coating thickness (μm)	Bondcoat material + thickness (mm)	Major phases or α-Al_2O_3 (%)	Vickers hardness
1	APS	St 37 1.5/5/10	$Al_2O_3 > 99.5$	420–510	NiAl 140–160	3–6.5	1250
2	APS	St 37 1.5/5/10	$Al_2O_3 > 99.5$	410–520	–	3–6.5	1250
3	APS	AISI 304 1.5/5/10	$Al_2O_3 > 99.5$	300–400	NiAl 100	3.5–6.5	1000
4	APS	AISI 304 1.5/5/10	$Al_2O_3 > 99.5$	310–360	–	3.5–6.5	1000
5	APS	Al alloy 1.5/5/10	$Al_2O_3 > 99.5$	320–380	NiAl 100–160	3.5–6	1100
6	APS	Al alloy 1.5/5/10	$Al_2O_3 > 99.5$	300–350	–	3.5–6	1100
7	APS	Copper alloy 1.5/5/10	$Al_2O_3 > 99.5$	320–370	NiAl 100–130	4–7	1150
8	APS	Copper alloy 1.5/5/10	$Al_2O_3 > 99.5$	300–340	–	4–7	1150
9	APS	Graphite 1.5/5/10	$Al_2O_3 > 99.5$	220	NiAl 20–30	3.5–6.5	1000
10	APS	Graphite 1.5/5/10	$Al_2O_3 > 99.5$	220–270	–	3.5–6.5	1000
11	APS	St 37 2 mm	Ni–5Al	200	–	Ni	220
12	APS	St 37 2 mm	Ni–5Al	400	–	Ni	220
13	APS	St 37 1.5 mm	$Al_2O_3 > 99.5$	50	–	5.5	1000
14	APS	St 37 1.5 mm	$Al_2O_3 > 99.5$	200	–	8.2	1000
15	APS	St 37 1.5 mm	$Al_2O_3 > 99.5$	450	–	7.5	1000
16	APS	St 37 1.5 mm	$Al_2O_3 > 99.5$	600	–	8.0	1000
17	HVOF	St 37 10 mm	WC–12Co	200, 400, 600, 770	–	WC	–
18	HVOF	St 37 1.5 mm	WC–12Co	15, 50, 200	–	WC	–
19	APS	St 37 2 mm	Inconel 625	100	–	Ni	200
20	HVOF	St 37 2 mm	Inconel 625	220	–	Ni	400
21	APS	St 37 1.5 mm	WC–12Co	330	–	WC	1050
22	HVOF	St 37 1.5 mm	WC–12Co	200	–	WC	1500
23	APS	St 37 2 mm	$Al_2O_3 > 99.5$	220	–	15	650
24	HVOF	St 37 2 mm	$Al_2O_3 > 99.5$	210	–	25	950

Table 4
Diffraction conditions and elastic constants for residual stress evaluation

Material	Radiation	Phase	Diffracting planes	2θ (°)	E (GPa)	ν	Penetration (μm)	
							63%	95%
Al_2O_3	Cu	γ-Al_2O_3	{844}	145.8	300	0.25	50	150
NiAl	Cu	Ni	{331}	144.7	224	0.29	10	30
Inconel 625	Cu	Ni	{331}	144.7	224	0.29	10	30
WC–Co	Fe	WC	{112}	145.5	700	0.20	2	6

Table 5
Coefficients of linear thermal expansion of coating and substrate materials used in the thermal stress estimation

Material	α ($\times 10^{-6}$ K^{-1})
Ferritic steel (substrate)	11
Alumina	7.58
WC–12%Co	5.5

The microstructure of the coatings was examined by optical metallography and by scanning electron microscopy (SEM), using equipment provided for EDS analysis. Phase structures were analysed by XRD, using Cu-Kα radiation. The detected diffraction lines were compared with reference lines of powder standards from the JCPDS map.

The apparent porosity of the coatings was determined by a volumetric method, for the APS samples, and by quantitative image analysis of the cross-sections, for those sprayed by HVOF.

3. Results and discussion

3.1. Microstructure of thermally sprayed coatings

Figs. 1 and 2 show micrographs of coatings produced by the two spraying processes. They are proposed to illustrate some important characteristics of the microstructure.

The main characteristic of the coatings is a lamellar structure of superposed and oriented layers, which is a result of the forming process. This feature is well illustrated by Figs. 1 and 2(a). In HVOF coatings it is not so well defined (Fig. 2b), because the increase of the impact velocity, in spite of the moderate heating, improves the cohesion and the density of the deposit. As a consequence of such a structure, discontinuities preferentially aligned parallel to the substrate surface are visible in the cross-sections of the coatings, clearly showing particular structures in the contact between sprayed particles. Regarding the spraying process, these characteristics are more marked in the APS coatings, thus revealing a weaker cohesion of these deposits.

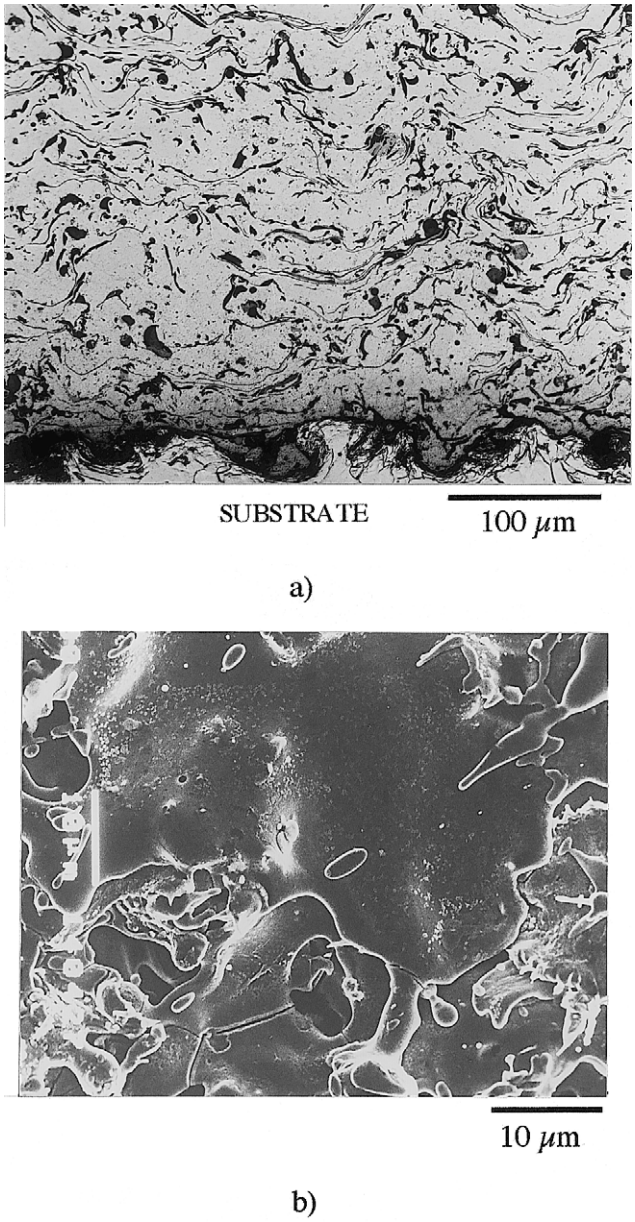

Fig. 1. (a) Cross-section of a NiAl APS coating, (b) microcrack within a splat observed at the surface of a WC–Co APS coating.

The porosities and voids typical of thermally sprayed coatings appear as dark spots in the micrographs of the cross-section, as shown by Fig. 1. By SEM observation

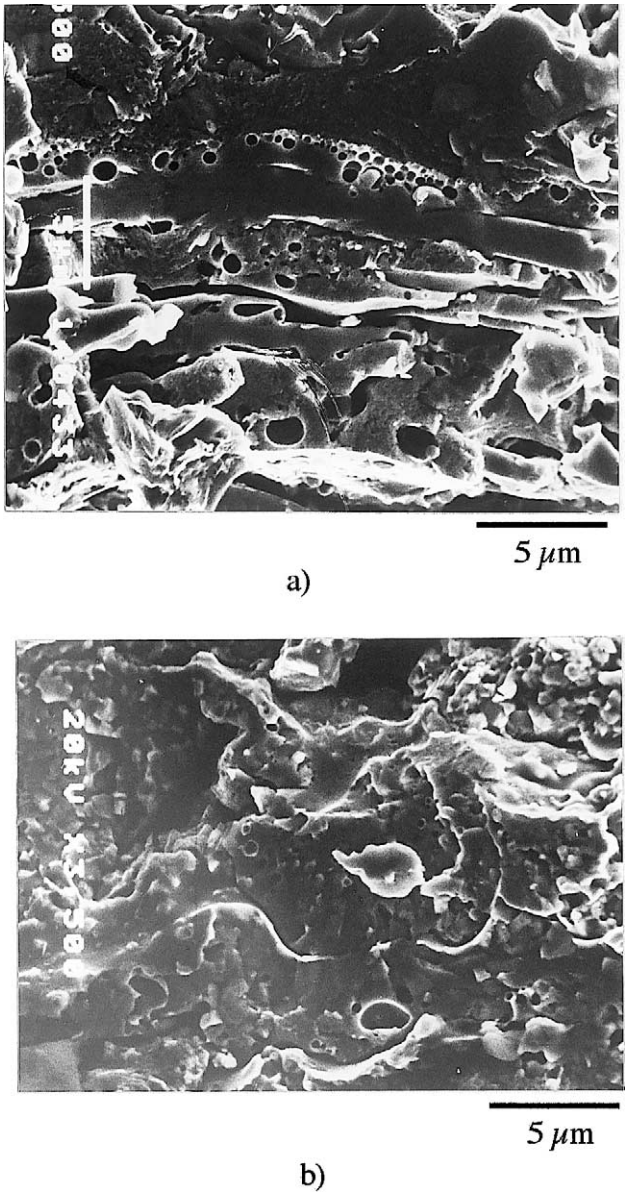

Fig. 2. SEM micrographs of the fracture surface of WC–Co coatings sprayed by: (a) APS, (b) HVOF.

their round or irregular forms can be recognised (Fig. 2). They are more common in APS than in HVOF coatings; this is explained by the higher temperature of the particles, because the pores may result from the evacuation of vaporised material during the solidification of the molten droplets.

Microcracks arise perpendicular to the surface and inside the lamellae of APS coatings, as shown by Fig. 1(b). They are explained by the release of quenching stress during spraying [4,6,23]. In HVOF coatings they are not (so clearly) observed.

3.2. Residual stresses and characteristics of the coating system

The residual stresses were evaluated in the surface layer of coatings adherent to the substrates. Layers of thickness conforming to the X-ray penetration were observed, as shown in Table 4. The study was carried out at several sites of each coating and the residual stresses were always determined along two perpendicular directions corresponding to azimuth angles of 0 and 90°. The results showed for each sample characteristics of a plane-equiaxial and tensile stress state, with constant values at sites far from the borders or irregularities. The results presented in the remainder of the study confirm this feature.

The level of the residual stresses in the top surface was related to characteristics of alumina coatings deposited by APS. The parameters considered were the substrate material (DIN St 37 K-ferritic steel, AISI 304-austenitic steel, aluminium alloy, copper alloy and graphite), the substrate thickness (1.5, 5 and 10 mm, for each material), and a bondcoat of NiAl (or its absence). The samples are listed in Table 3, numbered one to ten, and the results are shown in Fig. 3. As can be observed, the level of the residual stresses remains constant for all the samples inside the error bars. This behaviour can be related to the stress relief by extensive micro-cracking during spraying (Fig. 1b). The coating flaws, porosities and microcracks have an important effect on the stress release and only quenching stresses remain in the finished deposit.

This analysis is corroborated by the profile of residual stresses determined in the depth of some coatings deposited by APS. They show constant tensile stress values, inside the error bars, along the whole depth. No stress gradient is observed, neither in ceramic, nor in metallic coatings. Fig. 4 for NiAl and Fig. 5 for alumina are good examples of such results. They differ from the predictions of models based on the global heat transfer

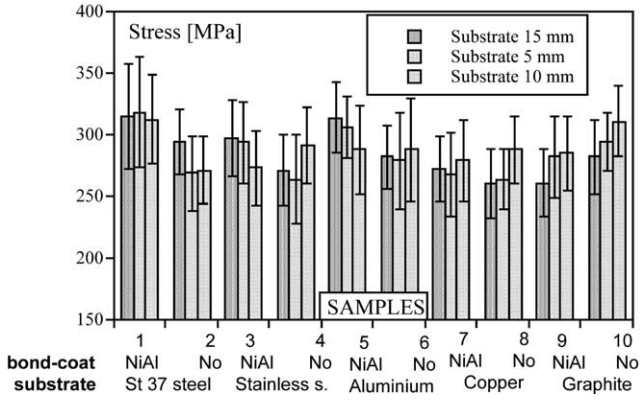

Fig. 3. Residual stresses in the surface layer (50 μm thick) of alumina coatings sprayed by APS on substrates of different materials and thicknesses, and with or without bondcoat.

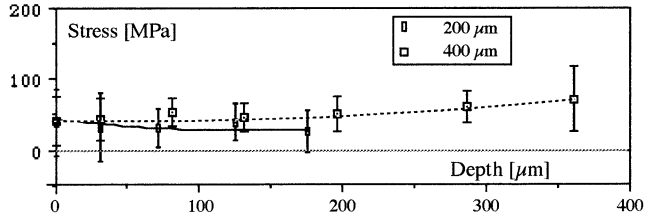

Fig. 4. Residual stresses in layers (10 μm thick) through-depth distributed in NiAl coatings with two different thicknesses, sprayed by APS (samples 11–12).

during the spraying process, which predict considerable gradients in the thickness of the deposits [15]. The residual stress state results only from the quenching stresses (Fig. 6a). The intensity is roughly constant in depth, because, as explained by Kuroda et al. [21], the steady-state value is a function of the characteristics of the impinging particles and the substrate temperature. This temperature reaches its maximum in a short time, if surface cooling is used during the process. Tensile values with similar profiles are predicted by a model developed by Gill and Clyne [24] for the effects of the quenching stresses.

On the contrary, a weak stress gradient is observed in WC–Co coatings, as exemplified in Fig. 7 for one sample 17 (200 μm thick at a 20 mm thick substrate). It can be explained by the superposition of cooling stresses to the quenching stresses. In the study of these coatings the effect of peening stresses mentioned by Kuroda et al. [2] was not observed. Cooling stresses are generated as a consequence of thermal mismatch strains in the interface coating-substrate, whose effects reach the surface, if the coating stiffness is high enough (Fig. 6b and c). This explains the increase of residual stresses with the deposit thickness observed on the surface of some coatings, as shown by Fig. 8. HVOF coatings denote the effect of the thermal energy accumulated during the spraying process, that is higher in the thicker deposits. In the industrial practice a higher probability of debonding is observed for the thicker deposits.

The effects of the cooling stresses can be detected on the results determined for the HVOF deposits which are denser and with lower amount of cracking than those sprayed by APS (Fig. 2). The explanation is corroborated by the comparison of results for the same material sprayed by both the techniques. These results, given in Table 6, show clearly that residual stresses reach higher values for the WC–Co HVOF coatings which are less porous than those deposited by APS. The exception of Al_2O_3 (samples 23–24) is justified by the higher amount of cracked α-Al_2O_3 observed in the HVOF sample. The residual stresses in this phase were close to zero.

3.3. Interpretation of the residual stress results

3.3.1. Quenching stresses

Quenching stresses are of a level that corresponds to the values determined in the top surface of free-standing coatings (Fig. 6a). They are always tensile and roughly constant through the deposit thickness. XRD data of quenching stresses, determined on the surface of different free-standing samples, are shown in Table 7.

3.3.2. Cooling stresses

The cooling stresses can be related to the effect of the coating-substrate connection by studying the residual stress relieving in free-standing coatings. For instance, the XRD data for WC–Co HVOF coatings given in Table 7 show higher values when the deposit is connected to the substrate than when it is free-standing. On the other hand, the alumina coatings have a different behaviour and the values remain constant, because of their brittleness, which induces mechanisms of strain accommodation inside the deposit.

The difference between the XRD data for the WC–Co HVOF coatings, before and after substrate removal, can be related to the cooling stresses generated in the

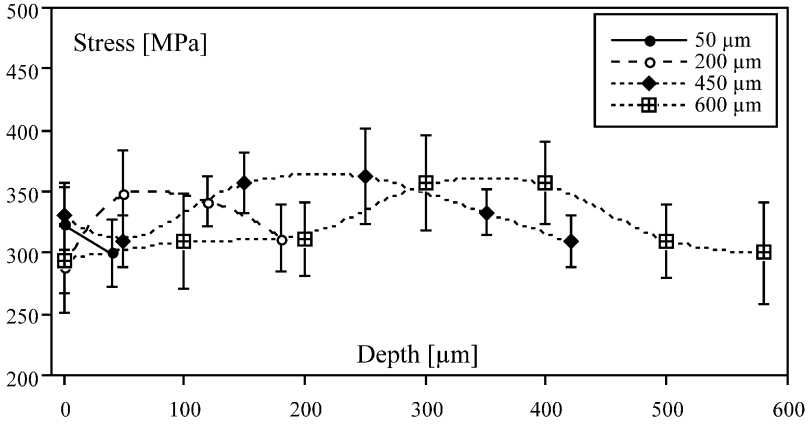

Fig. 5. Residual stresses in layers (50 μm thick) through-depth distributed in alumina coatings with four different thicknesses, sprayed by APS (samples 13–16).

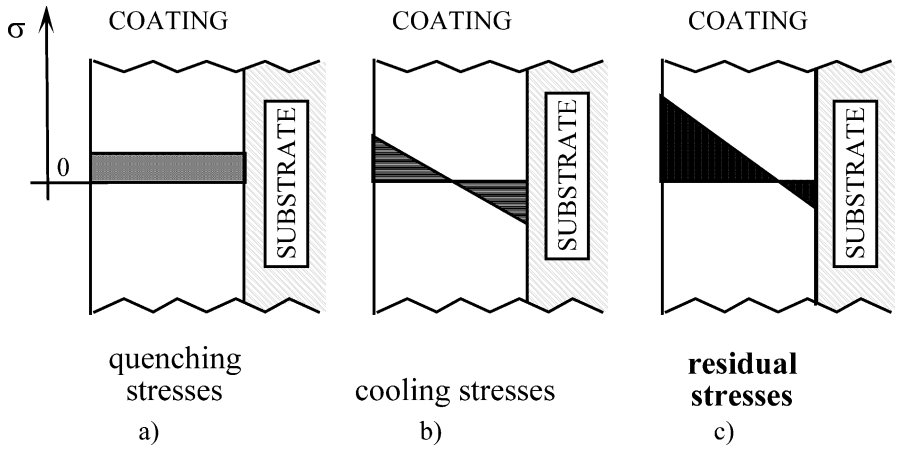

Fig. 6. Schematic explanation of residual stress generation in a thermal sprayed coating.

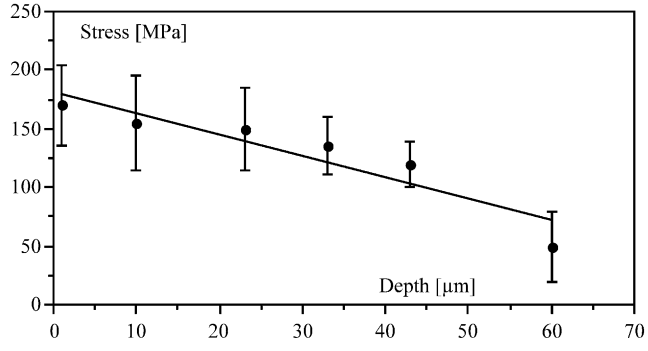

Fig. 7. Residual stresses in the depth of a WC–Co coating sprayed by HVOF.

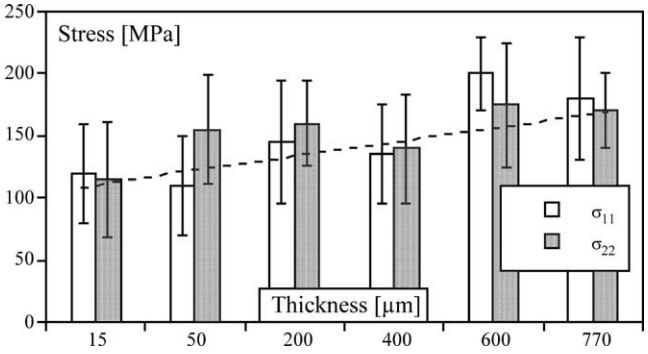

Fig. 8. Residual stresses in the surface layer (2 μm thick) of WC–Co coatings with different thicknesses, sprayed by HVOF (samples 17–18).

interface with the substrate as a consequence of thermal mismatch strains. In fact, the difference of the stresses determined in the surface layer of these samples is opposite in sign to the cooling stresses calculated for the coating at the interface with the substrate. They are representative of the maximum bending stress at the surface side of the coatings while they are connected to the substrates. These cooling stresses can be determined

Table 6
Comparison of surface residual stresses and porosities in coatings sprayed by APS and by HVOF

Sprayed material	APS		HVOF	
	σ_R (MPa)	Porosity (%)	σ_R (MPa)	Porosity (%)
Inconel (samples 19–20)	130±50	[a]	165±55	[a]
WC–12%Co (samples 21–22)	20±15	10	160±45	1
Al_2O_3 (samples 23–24)	410±60	10	190±25	<1

[a] Not measured.

by Eq. (1) or by the mechanical method based in the curvature radius of the free-standing coatings (Eq. (2)), if an approach by a fully elastic behaviour is assumed for the deposit. The results, given in Table 7, show that stresses calculated by Eq. (1) are compressive according to the relative magnitude of the thermal expansion coefficients of the coating and substrate materials. Also compressive, even though of lower level, are the values determined by Eq. (2), whose parameters of calculation are shown in Table 8. Both kinds of results, from Eq. (1) and from Eq. (2), agree with reasonable accuracy with the XRD data.

Cooling stresses, as responsible for a stress gradient in the coating thickness, explain the spalling of thick deposits of materials that can be affected by their action. Industrial practice shows that such a phenomenon occurs, not during the spraying process, but after some time has elapsed, during the cooling to room temperature. This is explained by the bending moment due to the stress gradient, which would reach considerable magnitude in the thickest coatings.

Table 7
Comparison between stress values determined by different methods

Samples	XRD residual stresses at the surface layer (MPa)			Cooling stresses [MPa]	
	Adhering	Free	Average difference	Eq. (1)	Eq. (2)
17–18	170±30	55±20	115	−135	−60
WC–12%Co	130±35	60±20	70	−170	−90
HVOF	160±45	75±30	85	−115	−100
23-Al_2O_3 APS	410±60	420±55	−10	−20	−3
24-Al_2O_3·HVOF	190±25	220±20	−30	−55	−17

Table 8
Samples and parameters used for the calculation of cooling stresses by the mechanical method

Samples	Thickness (mm)		E_C (GPa)	Average curvature radius (mm)
	Substrate	Coating		
17–18	10	0.21	140±20	230
WC–12%Co	10	0.40	175±25	380
HVOF	1.5	0.20	120±15	125
23–Al_2O_3·APS	2	0.22	30±10	1010
24–Al_2O_3·HVOF	2	0.21	90±20	545

4. Conclusions

The XRD method could be used to evaluate the residual stresses in thermally sprayed coatings. The experimental values are explained by the model theory that proposes two stages of stress generation: quenching stresses generated during the deposition of the sprayed particles, and secondary-cooling stresses generated during the cooling to room temperature. The residual stress state in the coating results from the superposition of both stresses, according to a damageable elastic behaviour.

The quenching stresses are due to the contraction of each molten particle during solidification. They are tensile and their magnitude is roughly constant along the depth of the deposit. This magnitude is close to the values determined by XRD in the surface of coatings detached from the substrate. Quenching stresses define the residual stress state of APS coatings where the dominant energy is of thermal origin. In this case residual stresses are insensitive to the coating thickness, substrate material and bondcoat.

The secondary-cooling stresses are due to the mismatch in thermal contraction between coating and substrate. Its magnitude can be estimated from the difference between XSE values in the surface layer of coatings adhering to the substrate and in free-standing coatings, as well as by the curvature radius of the last ones. They contribute to a stress gradient in dense coatings with a relatively high stiffness, because they are not affected by the release of quenching stress. In that case the secondary cooling component of the residual stress state increases with the coating thickness. The spalling of some thick coatings after spraying and during cooling to room temperature can be explained by the effects of the secondary cooling stresses.

Acknowledgements

This research was sponsored by financial support provided by FCT, the National Science and Technology Foundation. Thanks are due to CTCV-Technological Centre of Ceramic and Glass for spraying the specimens.

References

[1] L. Pawlowski, The Science and Engineering of Thermal Spray Coatings, Wiley, Chichester, UK, 1995, pp. 68–163.
[2] S. Kuroda, Y. Tashiro, H. Yumoto, S. Taira, H. Fukanuma, in: C. Coddet (Ed.), Proceedings of the 15th International Thermal Spray Conference, ASM International, Materials Park, Ohio, USA, 1998, pp. 569–574.
[3] R.C. Tucker, Jr, J. Vac. Sci. Technol. 11 (1974) 725–733.
[4] R. McPherson, Thin Solid Films 83 (1981) 297–310.
[5] R. McPherson, Thin Solid Films 112 (1984) 89–95.
[6] P. Fauchais, A. Grimaud, A. Vardelle, M. Vardelle, Ann. Phys. Fr. 14 (1989) 261–310.
[7] A. Ohmori, C.J. Li, Thin Solid Films 201 (1991) 241–252.
[8] M.J. Gudge, D.S. Rickerby, R. Kingswell, K.T. Scott, in: T.F. Bernecki (Ed.) Proceedings of the Third National Thermal Spray Conference, ASM International, Materials Park, Ohio, USA, 1990, pp. 331–337.
[9] J. Pina, A. Dias, J.L. Lebrun, Mater. Sci. Eng. A267 (1999) 130–144.
[10] S. Kuroda, in: Christian Coddet (Ed.), Proceedings of the 15th International Thermal Spray Conference, ASM International, Materials Park, Ohio, USA, 1998, pp. 539–550.
[11] H.W. Grünling, K. Schneider, L. Singheiser, Mater. Sci. Eng. 88 (1987) 177–189.
[12] S. Takeuchi, M. Ito, K. Takeda, Surf. Coat. Technol. 43/44 (1990) 426–435.
[13] Y.C. Tsui, T.W. Clyne, Thin Solid Films 306 (1) (1997) 23–33.
[14] D.S. Rickerby, G. Eckold, K.T. Scott, I.M. Buckley-Golder, Thin Solid Films 154 (1987) 125–141.
[15] R. Elsing, O. Knotek, U. Balting, Surf. Coat. Technol. 43/44 (1990) 416–425.
[16] R. Kingswell, K.T. Scott, B. Sorensen, in: S. Blum-Sandmeier, H. Eschnauer, P. Huber, A.R. Nicoll (Eds.), Proceedings of the

Second Plasma-Technik-Symposium, Plasma-Technik AG, Switzerland, vol. 3, 1991, pp. 377–388.
[17] D. Stöver, D.A. Jäger, H.G. Schütz, in: T.F. Bernecki (Ed.), Proceedings of the Fourth National Thermal Spray Conference, Pittsburgh, Pennsylvania, USA, May 4–10, 1991, ASM International, Materials Park, Ohio, USA, 1992, pp. 215–219.
[18] S. Kuroda, T. Fukushima, S. Kitahara, Vacuum 41 (1990) 1297–1299.
[19] S. Kuroda, T.W. Clyne, in: S. Blum-Sandmeier, H. Eschnauer, P. Huber, A.R. Nicoll (Eds.), Proceedings of the Second Plasma-Technik-Symposium, Plasma-Technik AG, Switzerland, vol. 3, 1991, pp. 273–283.
[20] T.W. Clyne, S.C. Gill, J. Therm. Spray Technol. 5 (4) (1996) 401–418.
[21] S. Kuroda, T. Dendo, S. Kitahara, J. Therm. Spray Technol. 4 (1) (1995) 75–84.
[22] S.C. Gill, T.W. Clyne, Metall. Trans. B 21B (1990) 377–385.
[23] S. Kuroda, T.W. Clyne, Thin Solid Films 200 (1991) 49–66.
[24] S.C. Gill, T.W. Clyne, Thin Solid Films 250 (1994) 172–180.
[25] J. Matejicek, S. Sampath, H. Herman, in: C. Coddet (Ed.), Proceedings of the 15th International Thermal Spray Conference, ASM International, Materials Park, Ohio, USA, 1998, pp. 419–424.
[26] K. Tanaka, K. Suzuki, R. Kawase, in: H. Fujiwara, T. Abe, K. Tanaka (Eds.), Proceedings of the International Conference on Residual Stresses 3 (ICRS3), Elsevier Applied Science, London, vol. 1, 1992, pp. 704–709.
[27] H.D. Tietz, B. Mack, St. Böhm, in: Proceedings of the Fourth International Conference on Residual Stresses (ICRS4), Society for Experimental Mechanics, Inc, Bethel, USA, 1994, pp. 654–661.
[28] M. Nishida, T. Hanabusa, in: T. Ericsson, M. Odén, A. Andersson (Eds.), Proceedings of the Fifth International Conference on Residual Stresses (ICRS5), Institute of Technology, Linköping, Sweden, vol. 2, 1997, pp. 1018–1023.
[29] D. Dantz, C. Genzel, W. Reimers, K.-D. Liss, in: Proceedings of the Sixth International Conference on Residual Stresses (ICRS6), IOM Communications Ltd, London, UK, vol. 1, 2000, pp. 717–724.
[30] M. Nishida, T. Hanabusa, in: Proceedings of the Sixth International Conference on Residual Stresses (ICRS6), IOM Communications Ltd, London, UK, vol. 2, 2000, pp. 1084–1091.
[31] D.J. Greving, E.F. Rybicki, J.R. Shadley, J. Therm. Spray Technol. 3 (4) (1994) 379–388.
[32] I.C. Noyan, J.B. Cohen, Residual Stress-Measurement by Diffraction and Interpretation, Springer, New York, 1987, pp. 134–135.
[33] J.H. Hubbell, W.H. McMaster, N.K. Del Grande, J.H. Mallett, X-Ray cross-sections and attenuation coefficients, in: J.A. Ibers, W.C. Hamilton (Eds.), International Tables for X-ray Crystallography, Kynoch Press, Birmingham, England, 1974, pp. 47–66.
[34] J. Li, Z. Kang, Z. Wang, in: H. Fujiwara, T. Abe, K. Tanaka (Eds.), Proceedings of the Third International Conference on Residual Stresses (ICRS3), Elsevier Applied Science, London and New York, vol. 2, 1992, pp. 1007–1012.
[35] M. François, J.M. Sprauel, C.F. Déhan, M.R. James, F. Convert, J. Lu, J.L. Lebrun, N. Ji, R.W. Hendricks, X-Ray diffraction method, in: J. Lu (Ed.), Handbook of Measurement of Residual Stresses, Society for Experimental Mechanics, USA, 1996, pp. 71–131.
[36] R.W. Hoffman, in: G. Hass, R. Thun (Eds.), Physics of Thin Films, vol. 3, Academic Press, New York, 1966, p. 211.
[37] A. Tronche, P. Fauchais, Mater. Sci. Eng. 92 (1987) 133–134.
[38] S. Rangaswamy, H. Herman, S. Safai, Thin Solid Films 73 (1980) 43–52.
[39] H. Nakahira, K. Tani, K. Miyajima, Y. Harada, in: C:C: Berndt (Ed.), Proceedings of the 13th International Thermal Spray Conference and Exposition, ASM International, Materials Park, Ohio, USA, 1992, pp. 1011–1017.